Science Advances

AAAS

advances.sciencemag.org/cgi/content/full/4/3/eaao7051/DC1

Supplementary Materials for

Poro-elasto-capillary wicking of cellulose sponges

Jonghyun Ha, Jungchul Kim, Yeonsu Jung, Giseok Yun, Do-Nyun Kim, Ho-Young Kim

Published 30 March 2018, *Sci. Adv.* **4**, eaao7051 (2018)
DOI: 10.1126/sciadv.aao7051

The PDF file includes:

Other Supplementary Material for this manuscript includes the following:

(available at advances.sciencemag.org/cgi/content/full/4/3/eaao7051/DC1)

- movie S1 (.mov format). Wicking and swelling in the cellulose sponge.
- movie S2 (.mov format). The merging of micropores in the cellulose sheets.

section S1. Effects of isotropic volumetric expansion on liquid rise height

The cellulose sponge swells isotropically by absorbing water or aqueous solutions, but it should match the size of the upper dry region near the wet-dry interface. The region of such deformation (white curved line in Fig. 3A of the main text), whose length is approximately 2 mm, is relatively small compared to the rise height h and Jurin's height h_J, which allows us to simplify the model as illustrated in Fig. 3D.

In the vertical direction, the total wet distance H from the bottom of the sponge to the wet front is related to the measured rise height h by $h = H/(1+\varepsilon_s)$. The liquid flux that enters the initially dry region of the cross-sectional area A_d, uA_d, contributes to the transverse expansion causing the area to increase from A_d to $A_w = A_d(1+\varepsilon_s)^2$ as well as to the rise of the wet front $\dot{H}$. Hence, we write $uA_d \approx \dot{H}A_w$, which leads to $\dot{H} \approx u/(1+\varepsilon_s)^2$.

section S2. Correlation between hygroscopic strain and pore coalescence

We consider a thin perforated sheet with N_0 pores, which is stretched isotropically in its plane. As demonstrated in movie S2 which actually employs a biaxial extension due to the limit of experimental setup, the growing holes approach each other until they merge to form a larger pore. We observe similar coalescence process of micropores in the cellulose sheet as it becomes wet in Fig. 2D of the main text. The similarity between the stretched perforated membrane and hygroscopically expanding porous sheet is discussed below. Our theory requires a simple relationship between the hygroscopic strain ε and the change of pore numbers via merging, or $N_0/N = f(\varepsilon)$ with N_0 and N being the number of pores before and after coalescence. Because the change of pore numbers via coalescence has been seldom treated theoretically, we employ an experimental approach to empirically find the functional form of $f(\varepsilon)$.

As shown in fig. S2A, we start with thin PDMS (polydimethylsiloxane) films 100 μm in thickness with dozens of holes of the radius a = 2 mm. We stretch the films in the two perpendicular directions using two linear stages (M-IMS300LM, Newport) as shown in fig. S2B and C. We count the number of pores as the strain increases to obtain N_0/N as a function of ε. The results are displayed in fig. S2D, where the number ratio linearly increases with ε once the strain reaches the threshold value. The value is different for each perforation condition, which also affects the slope of the straight lines. Although the hole radii were identical for all the films, their spacings were different. Figure S2E and F show the probability of the inter-pore distance d scaled by a for the two extreme cases, films 1 and 5. When the inter-pore distance is densely distributed in the range of very small values as in film 1, the threshold strain over which N_0/N begins to increase is close to zero and the increase rate (slope of the line) is large. For films with relatively large inter-pore distances as in film 5, the threshold strain is relatively large and the line slope is small.

Our measurement result of inter-pore distance of micropores in the cellulose sheet is displayed in fig. S1C. It clearly shows that the pores are rather densely spaced, so that the inter-pore distance probability resembles that of film 1 in fig. S2E. Therefore, we assume

$N_0/N \approx 1+ \beta\varepsilon$ for the cellulose sheet. We empirically find β based on the number of pores of a cellulose sheet before (N_0) and after (N) wetting in the ESEM chamber and the hygroscopic strain ($\varepsilon \approx 0.23$). As a result of three runs, we obtain $\beta \approx 50 \pm 7.7$, which further allows us to estimate $N_0/N \approx \beta\varepsilon$ for $\beta\varepsilon >> 1$.

While physical mechanisms causing stress and strain in stretched membranes and hygroscopically expanding sheets are different, the resultant deformation patterns are similar. To illustrate the similarity, we perform finite element analysis (FEA) for a circular sheet with two and four holes to compare the deformation patterns under tension and hygroscopic pore expansion using the commercial FEA program, ADINA version 9.3. Sheet stretching is simulated by imposing a radial force uniformly distributed along the outer boundary of the sheet (fig. S3A). To model the case of hygroscopic pore expansion, a thin circular layer of high moisture content is introduced near the pore boundary. This is a simple model for what happens in the actual wicking experiments, where the water that enters a micropore diffuses outward from the pore boundary while keeping the water content near the boundary very high. In the ESEM experiments, the moisture flux from the ambient humid air is maximized at the pore boundary as computed in fig. S4, allowing us to assume a high moisture content near the pore boundary.

As seen in fig. S3B, these two different models provide similar deformations. First of all, the radius of holes increases but the distance between adjacent pore boundaries decreases, which causes necking of the sheet between two pores that would lead to pore coalescence. The effective, von Mises stress (often used in failure criteria of materials) is localized near pores, particularly at the pore-pore interface, due to stress concentration. Notably, it is dominated by the positive (tensile) hoop stress (the stress component defined in the circumferential direction of pores) responsible for pore expansion. The rupture or cracking of pores is likely to be initiated by these highly tensile stress components particularly in the necking region between pores. These results clearly demonstrate that pore deformation characteristics in the two situations are similar, suggesting that our biaxial stretching experiment can closely emulate the pore coalescence phenomenon in the actual hygroscopic expansion of porous sheets.

section S3. Recovery of microporous structure of cellulose sponges

To test whether microporous structure of cellulose sponges is recovered after repeated cycles of wetting and drying, we took scanning electron microscopy (SEM) images of dry cellulose sponges that had undergone saturation and drying cycles with water. As shown in fig. S5, the microporous structures are similar regardless of the number of cycles of wetting and drying.

section S4. The volume fraction of aqueous liquid in a cellulose sheet

The volume fraction of an aqueous liquid in a cellulose sheet, η, is given by $\eta = V_l/V_c$, where V_l and V_c are the volumes of the liquid and the cellulose, respectively. In fig. S6a, we see that the cellulose volume $V_c = V_t - V_p$, where V_t and $V_p \sim N_0 r_0^2 s$ are the total volume and micropore volume, respectively. Since the porosity of the sheet $\phi = V_p/V_t$, we obtain $V_c \sim (1-\phi)N_0 r_0^2 s/\phi$.

The image analysis as illustrated in fig. S6b gives $\phi \approx 0.47$. The diffusion length $l_d \sim (Ds/u)^{1/2} \sim 0.1$ μm is very small compared to the micropore radius $r_0 \sim 1$ μm for the typical wicking velocity $u \sim 0.1$ mm/s in the late stages. Thus, we write $V_l \sim N_0 r_0 l_d$, which finally leads to $\eta \sim \phi l_d/(1-\phi)/r_0$.

section S5. Effects of water concentration on hygroscopic strain

In our experiments to induce hygroexpansion of sponges, we used not only water but also aqueous liquids, i.e. glycerin and ethylene glycol mixed with water at different weight ratios, to check the validity of our theory for a wide range of liquid properties, such as density, viscosity, and surface tension coefficient. We measured the maximum (or saturated) hygroscopic strain, ε_s of cellulose sponges for various aqueous liquids independently of the capillary rise experiments. The results, displayed in fig. S7, show that the values of ε_s for various liquids is nearly identical to the value for pure water when the weight content of water is over 20%. Thus, we use $\varepsilon_s = 0.23$ for all the liquids in this work, which leads to $\alpha \approx 0.33$.

section S6. Mechanical properties of cellulose sponges

We measured Young's modulus of the present cellulose sponges by using a tensile testing machine (Instron 5543). To obtain Young's modulus of the solid part except pores, we introduce a linearized empirical relationship (*36*), $E = E_0(1-\Phi)$ where E and E_0 are Young's modulus of porous material and solid part, respectively, and Φ is the macroscale bulk porosity ($\Phi \approx 0.9$). We use Poisson's ratio $\nu = 0.30$ following Ref. (*26*). The shear modulus is given by $G = E_0/(1+\nu)/2$. The elastic modulus decreases as the cellulose sponge absorbs water as shown in fig. S8. As the shear modulus of a wet porous medium appearing in the expression of diffusivity, we used $G = 1.62$ MPa.

section S7. Capillary rise in pre-swollen sponges

To test the effects of hygroscopic swelling on capillary rise dynamics, we measured the rise height of water in a sponge which had been swollen by water vapor without its micro and macro voids filled with the liquid. Figure S9 shows that the water rise height grows like $t^{1/4}$ in the late stages in pre-swollen sponges, while it grows like $t^{1/5}$ in unsaturated sponges. This result indicates the critical role of the hygroscopic swelling in the capillary rise dynamics in the late stages. The inset of fig. S9 shows that the power law of the rise height follows Lucas-Washburn's rule ($t^{1/2}$) regardless of liquids in the early stages.

section S8. Scaling laws of water rise within bread made from starch

Starch, the most common carbohydrate in human diets, is a polymeric carbohydrate that swells with absorbing water just as cellulose. To observe water wick against gravity in a bread made from starch, we placed an initially dry bread on a water bath as shown in fig. S10A. The measurement results of the rise height reveals that h grows like $t^{1/2}$ in the early stages and $t^{1/5}$ in the late stages, fig. S10C, which agrees with the power laws observed with cellulose sponges. Pores of bread were found to coalesce while impregnated with water as shown in fig. S10B, the similar behavior seen in the cellulose sponges.

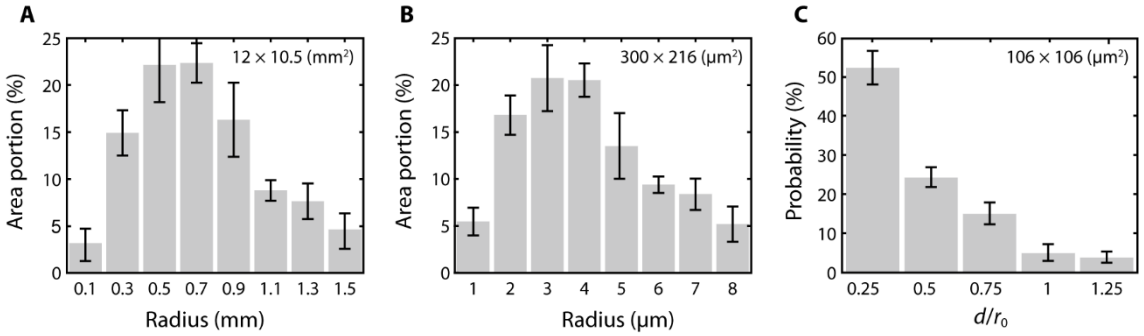

fig. S1. The measurement data of the cellulose sponge structure. (**A**) Optically measured areal density of macropores. (**B**) Areal density of micropores measured with SEM images. The error bars of the data correspond to the standard deviation of the average pore radii of three samples. (**C**) Inter-pore distance distribution of the cellulose sheets. The error bars of the data correspond to the standard deviation of the average inter-pore distance of six samples. The area of measurement is specified in each plot.

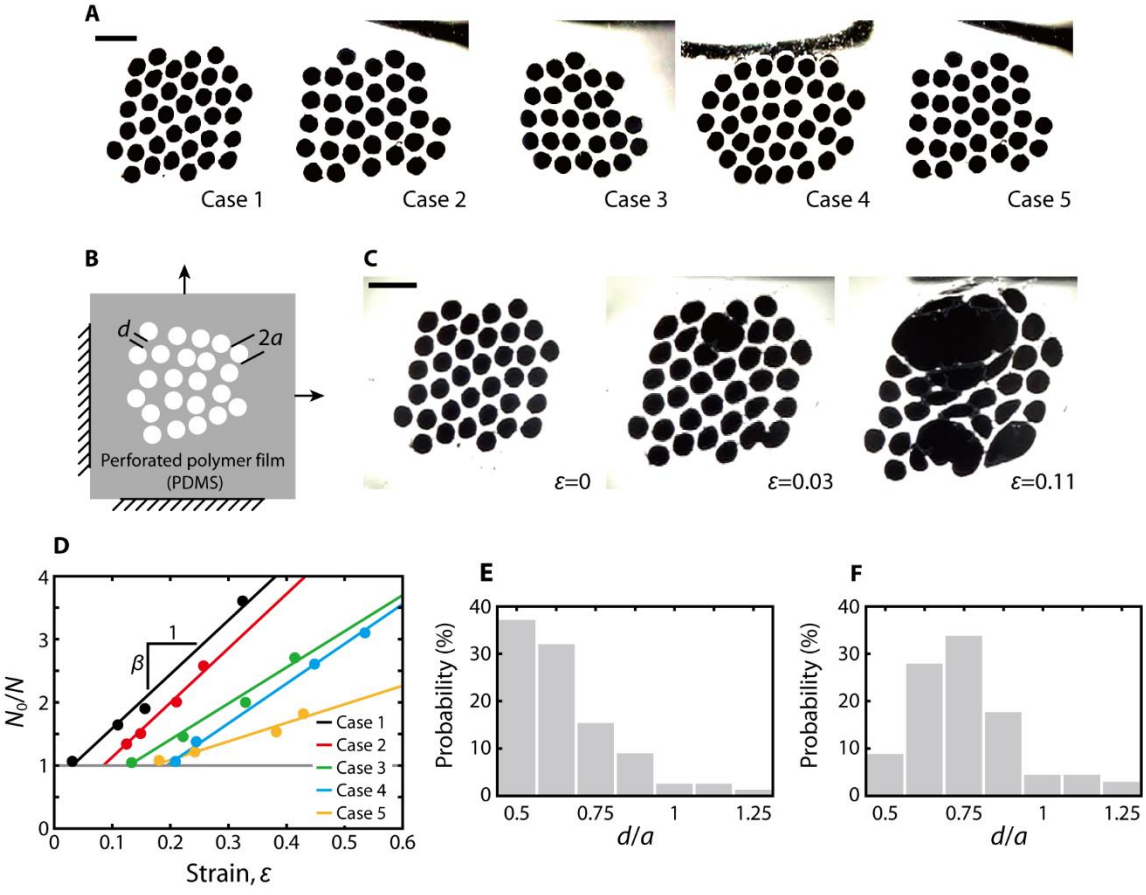

fig. S2. Macroscopic experiments for pore coalescence. (**A**) Perforated thin polymer films (initial state). The radius of pores, a, is 2 mm. Scale bar, 10 mm. (**B**) A schematic of experimental setup. The left and bottom sides are clamped, and the right and upper sides of the film are pulled by the linear stages. (**C**) Experimental images of the pore coalescence (case 1). Scale bar, 10 mm. (**D**) The number ratio N_0/N versus strain ε. The coalescence tends to occur quickly when β is high. Dimensionless inter-pore distance (d/a) distribution of case 1 (**E**) and case 5 (**F**).

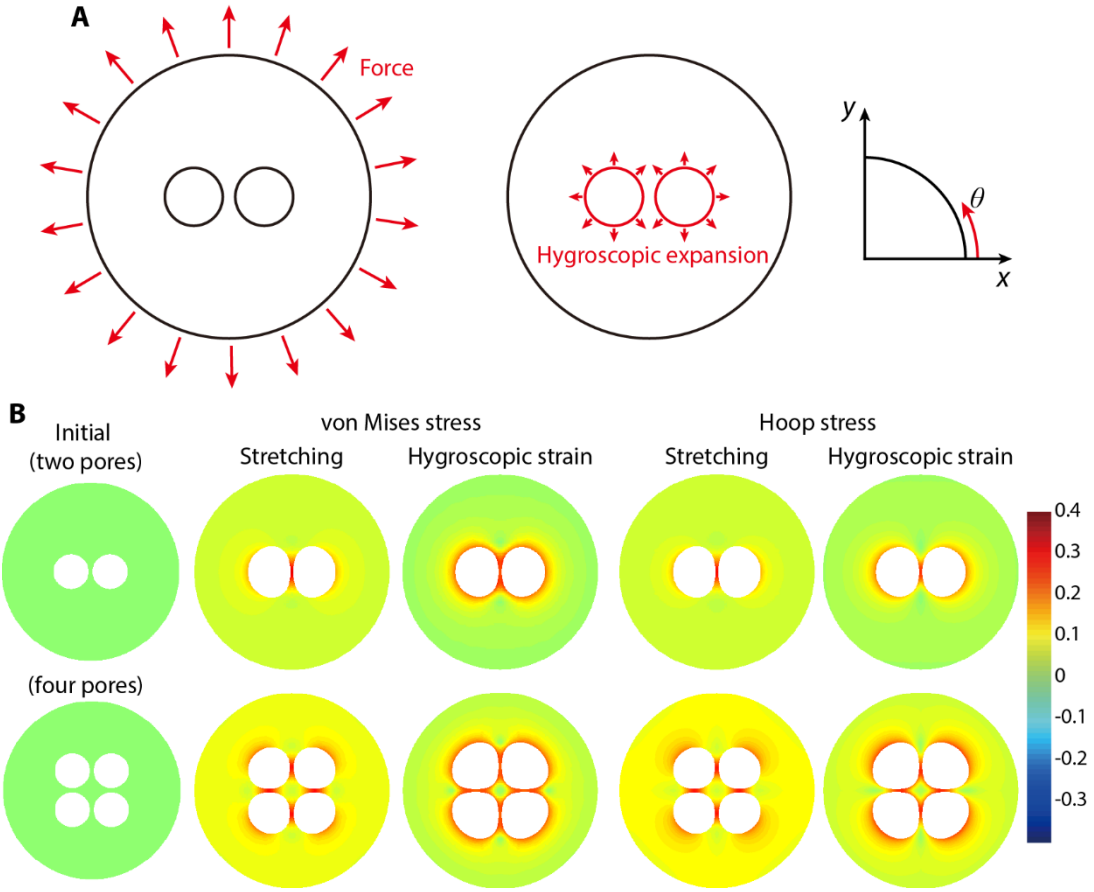

fig. S3. Numerical analysis of porous sheet deformation. (A) The loading conditions for finite element models. Left: external stretching. Right: hygroscopic swelling. (B) Von Mises stress and hoop stress distribution of stretching and hygroscopic swelling models. The hoop stress is defined by the stress along the θ-θ direction with the origin of cylindrical coordinate located at the center of individual pores. The color bar indicates the relative stress.

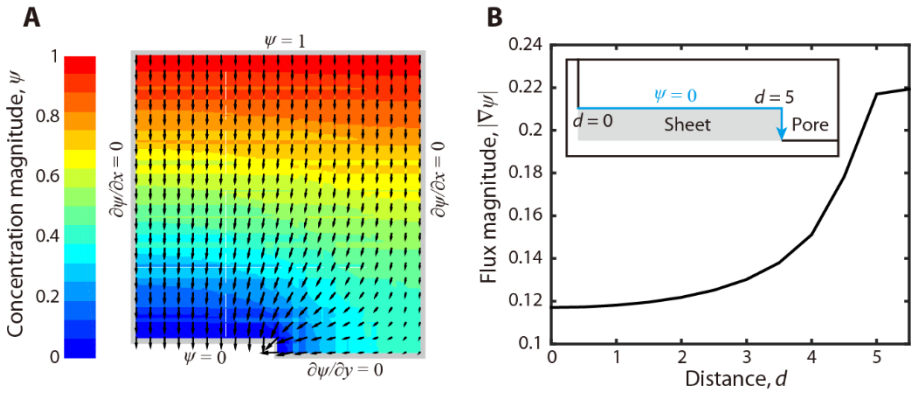

fig. S4. Moisture flux into cellulose sheet in ESEM chamber. (A) Numerical computation results of the moisture concentration (ψ) distribution based on the steady diffusion model, $\nabla^2\psi = 0$, with the boundary conditions specified in the figure. Black arrows indicate the orientation of the flux. (B) Flux magnitude versus distance along the blue line (inset). The flux is very high near the boundary between the sheet and the pore at $d = 5$.

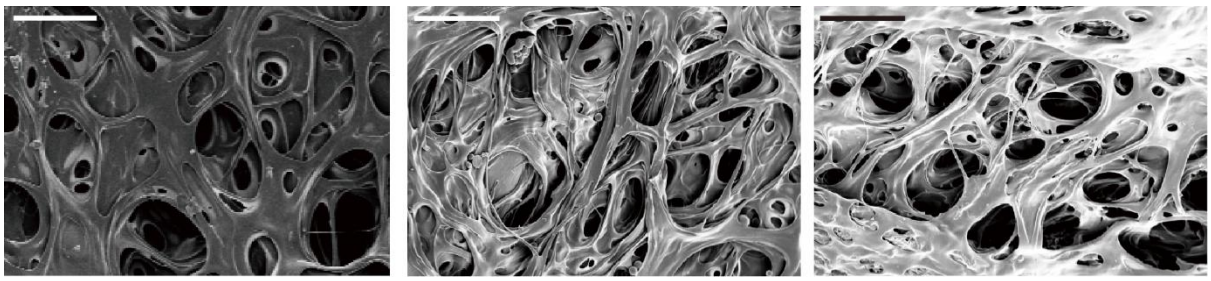

fig. S5. Microporous structure of cellulose sponges after cycles of wetting and drying with water. From left to right, SEM images of sponge after 0, 5, and 10 cycles. Similar microporous structure is observed although different specimens are used for microscopy due to experimental limits. Scale bar, 10 μm.

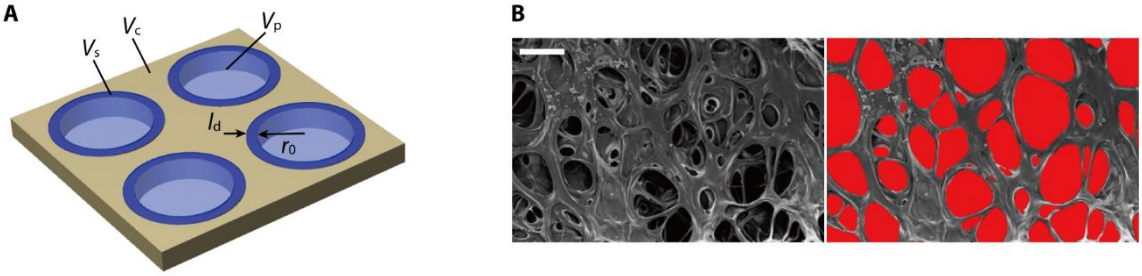

fig. S6. Analysis of the cellulose sheets. (**A**) A schematic of liquid diffusion in a wet microporous cellulose sheet. (**B**) SEM image (left) and post-processing image (right). We calculated the area fraction of pores (red area) to measure the porosity of a sheet. Scale bar, 10 μm.

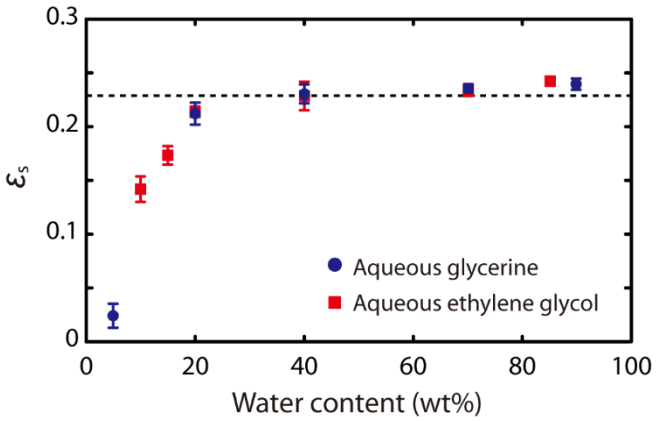

fig. S7. Hygroscopic strain of saturated sponge for different water contents in aqueous glycerin and ethylene glycol. The error bars of the data indicate the standard deviation of the average hygroscopic strain of four measurements at each weight concentration.

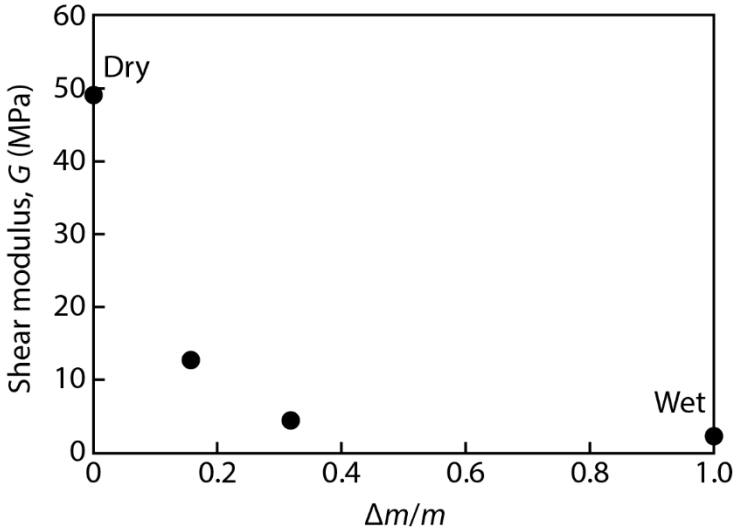

fig. S8. Shear modulus of dry and wet cellulose sponge. The shear modulus calculated from the measurement results of Young's modulus for different water concentration, $\Delta m/m$, where Δm is the mass of water and m is the mass of initially dry sponge. The error bar is smaller than the size of the symbols.

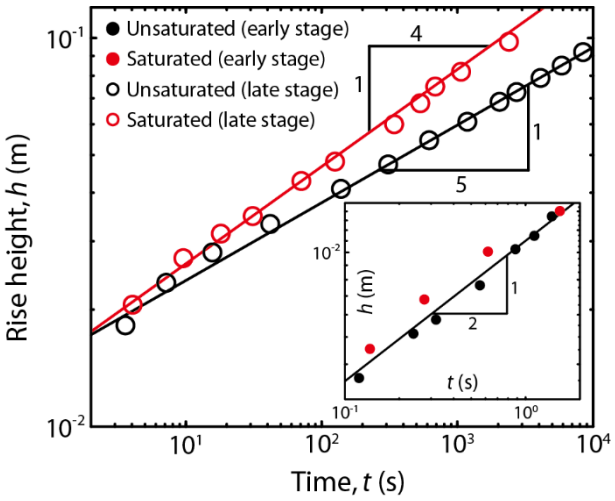

fig. S9. Capillary rise height of water versus time in an initially dry sponge (black) and pre-swollen sponge (red). In the late stages, the rise height grows like $t^{1/4}$ in the pre-swollen sponge while it follows the $t^{1/5}$ law in the initially dry sponge. Inset: In the early stages, the rise heights of the both saturated and unsaturated sponges follow the $t^{1/2}$ rule.

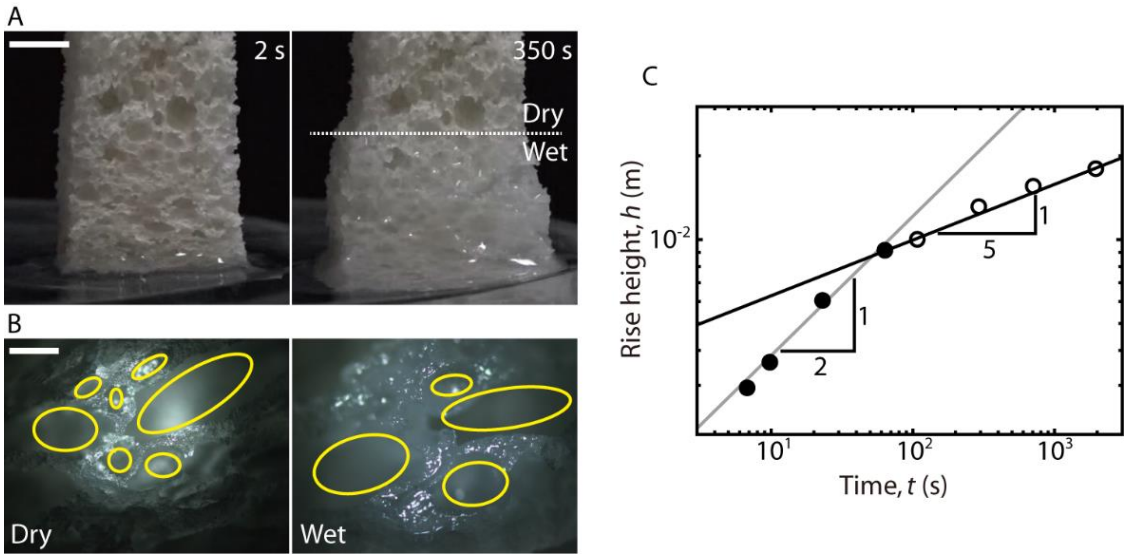

fig. S10. Capillary rise in porous bread. (**A**) Optical images of water wicking in initially dry bread. Scale bar, 5 mm (**B**) Merging of pores with water impregnation as imaged by an optical microscope. Scale bar, 30 μm. (**C**) The rise height of water versus time. In the early stages (filled symbols), the rise height grows like $t^{1/2}$ (gray line). In the late stages (open symbols), the rise height follows the $t^{1/5}$ rule (black line).

table S1. List of liquid properties and symbols. Physical properties of water, aqueous glycerin (*37*), aqueous ethylene glycol (*38*), turpentine and silicone oils at 23°C, and symbols for the liquids.

Liquid	Symbol		Viscosity, μ (Pa·s)	Density, ρ (kg/m^3)	Surface tension, γ (N/m)	Diffusivity, D (10^{-11} m^2/s)
	Early	Late				
Water	●	○	0.001	998	0.072	17.72
Glycerine 30 wt%	★	☆	0.0022	1071	0.069	8.05
Glycerine 60 wt%	◆	◇	0.009	1151	0.068	1.97
Glycerine 80 wt%	▲	△	0.047	1205	0.065	0.38
Ethylene glycol 30 wt%	▼	▽	0.0017	1033	0.061	10.43
Ethylene glycol 60 wt%	◀	◁	0.0038	1067	0.055	4.66
Ethylene glycol 80 wt%	▶	▷	0.0068	1090	0.050	2.61
Turpentine	■	□	0.0014	870	0.027	-
Ethylene glycol 99 wt%	×	-	0.018	1112	0.048	-
Silicone oil I	+	-	0.10	970	0.020	-
Silicone oil II	*	-	1.00	970	0.020	-

movie S1. Wicking and swelling in the cellulose sponge. The movie plays at 32X real-time speed. The cellulose sponge swells while being wetted.

movie S2. The merging of micropores in the cellulose sheets. The movie plays at 64X real-time speed. As the cellulose sheets absorb the water in the humid ESEM chamber, the pores expand, and then merge to form larger pores.